Virtual Friction Control for Power System Oscillation Damping with VSC-HVDC Links

Alberto Rodríguez-Cabero*, Javier Roldán-Pérez*, Milan Prodanovic*, Jon Are Suul†, Salvatore D'Arco†

*IMDEA Energy Institute, Madrid, Spain. †SINTEF Energy Research, Trondheim, Norway.

{alberto.rodriguez, javier.roldan, milan.prodanovic}@imdea.org, {jon.a.suul, salvatore.darco}@sintef.no

Abstract—This paper presents a technique for damping of oscillations in ac grids by control of VSC-HVDC links. The effect of the proposed controller is equivalent to a mechanical friction between two asynchronous networks (modelled as rotating masses) interconnected by the HVDC link. Therefore, the dynamics of the ac grids will be coupled, and the virtual friction gain can be utilised to effectively damp frequency oscillations in any of the ac networks. A centralised and a decentralised implementation of the proposed controller are presented. It is shown that both implementations of the virtual friction-based damping can effectively attenuate poorly damped frequency oscillations in both of the interconnected ac grids and that the decentralised implementation can ensure damping without relying on fast communication between the HVDC terminals. The impact of the proposed controller on the stability of the two grids is analysed with a simplified system model, and the performance is experimentally validated by a scaled laboratory setup.

I. INTRODUCTION

Power and frequency oscillations are well-known power system issues that have been studied for decades [1]. In traditional power systems, the large inertia provided by synchronous generators helps stabilising the system frequency [2]. However, any given synchronous generator can oscillate around its steady-state position, producing local oscillatory modes [3]. These electro-mechanical oscillations are largely defined by the inertia of synchronous generators, the governors and the topology of the power system [1]. While the potential sources of oscillations in traditional power systems are well established, modern power systems are increasingly integrating Renewable Energy Sources (RES) with power electronic grid interfaces [4]. These power converters do not behave as conventional generators, and do not inherently provide inertial response or similar transient dynamics as synchronous machines [5]. Therefore, new oscillatory problems related to the gradually increasing penetration of RES and power electronic converters are considered as critical issues for power system operation.

Stability of electrical grids interconnected by HVDC link has been thoroughly investigated in the last decades [6]. The initial research efforts within this area were focused on Current

Source Converters (CSC) HVDC links [3]. However, most recent research activities are focused on utilization of VSC-HVDC systems for improving the stability of power systems and for damping of power and frequency oscillations [7–9]. To mitigate the impact of the declining equivalent inertia of power systems, some authors have proposed specific control strategies that emulate the dynamic properties of synchronous generators [10–13]. This is an attractive approach since power systems are inherently designed to operate with synchronous generators. However, in most cases, this approach implies that the dc-voltage regulation has to be in the same time-scale as the synchronous machine dynamics, and this can threaten the dc voltage stability.

Several control strategies have also been proposed for utilizing HVDC-links to damp oscillations in emerging power system configurations. For example, Zeni *et al.* [8] recommended guidelines for controller design in order to damp oscillations in HVDC links connected to off-shore wind-farms. In [14] a supplementary controller based on neural networks was introduced for inter-area Power Oscillation Damping (POD). The method provides accurate results, but it is computationally intensive. Other authors focused on control strategies for POD by using Wide Area Measurement Signals (WAMS). For example, Pierre *et al.* [15] proposed a supervisory controller for inter-area POD by using real-time frequency measurements, while Agnihotri *et al.* [16] designed a robust controller that considered the loss of communications. These controllers showed satisfactory performance, but the requirement of fast communication reduces the reliability. Other authors have proposed the use of the dc-link voltage as an indicator of the ac network frequency deviation, avoiding the use of high bandwidth communications. One of the first attempts was introduced by Phulpin [17], who proposed a communication-free control scheme that allowed offshore wind generators connected through VSC-HVDC links to provide inertia. Recently, several authors have proposed control strategies to provide frequency support and inertia emulation via a coordinated dc-link voltage regulation [18, 19]. However, these control strategies cannot be used to damp local oscillation modes.

This paper introduces a controller that emulates an electro-mechanical friction between two ac grids interconnected via a VSC-HVDC link. The proposed controller is based on a representation of the link in terms of differential and common power [20] and two alternative control implementations are proposed. The first implementation relies on a centralised
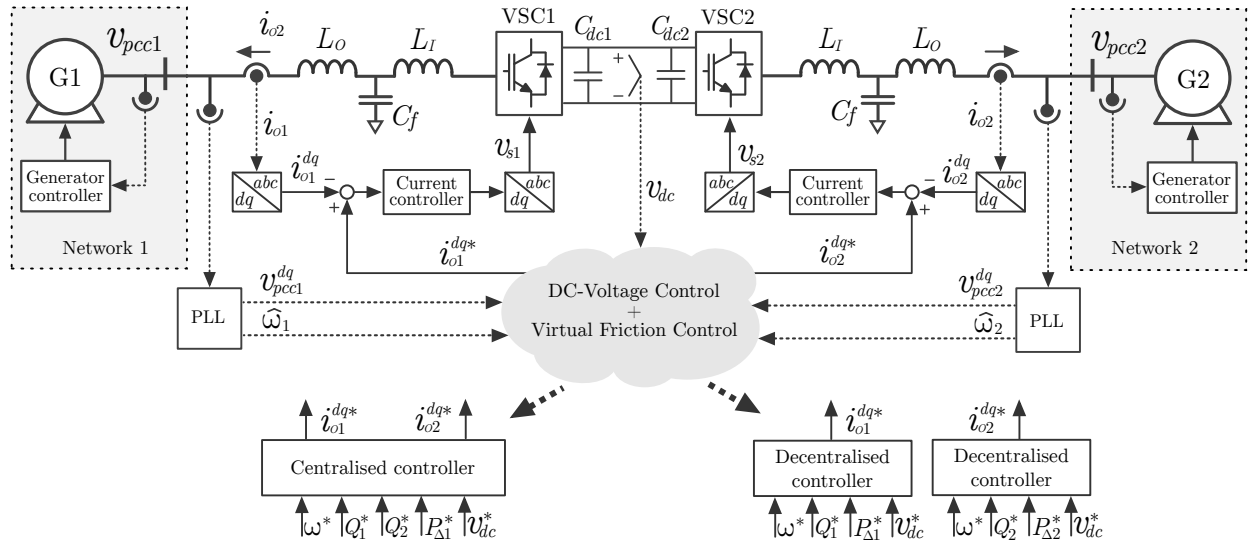
Fig. 1. Electrical and control diagram of a point-to-point link that provides virtual friction and voltage support to both sides of the link.

controller, and the local measurements of both terminals are used in real-time for the damping control. The second implementation is a decentralised version where two identical controllers are applied at each terminal without depending on a fast communication. The POD capability of the proposed controller is analytically evaluated by using a simplified model of two ac networks. Finally, the performance of the control scheme is experimentally validated by a scaled laboratory prototype of the VSC-HVDC link.

II. SYSTEM OVERVIEW AND MODELLING

A. Application Description

Fig. 1 shows the electrical and control system diagram of the point-to-point VSC-HVDC link studied in this paper. It consists of two VSCs (VSC1 and VSC2) that interconnect two independent electrical networks represented by two equivalent synchronous generators (G1 and G2, respectively). The HVDC-link terminals operate as power-controlled sources that can inject or absorb active and reactive power from the ac grids. For each terminal, the grid-side current is i_o, v_s is the VSC output voltage, and v_{dc} is the dc-capacitor voltage. The terminal (1 or 2) is marked in the subscript of variables (i.e. i_{o1}). The dc capacitor of each VSC is C_{dc} (C_{dc1} and C_{dc2}), and $C'_{dc} = C_{dc1} + C_{dc2}$.

Two alternatives for the proposed controller are introduced in this paper:

1) In the first implementation, measurements of both sides of the link are used in real-time. Therefore, fast communication between control systems is assumed. This approach can for instance be applicable in back-to-back interconnections between asynchronous networks.
2) For the second implementation, the control system is divided into two identical controllers (one for each terminal) that can be implemented in different control platforms without the use of communications between

terminals. This approach is intended for long distance HVDC transmission systems.

B. Common and Differential Power Concepts

The differential- and common-power representation of the point-to-point HVDC link is defined as follows [20]:

$$p_{cm} = -(p_{o1} + p_{o2}), \qquad (1)$$
$$p_\Delta = (p_{o1} - p_{o2})/2, \qquad (2)$$

where p_{o1} and p_{o2} are the instantaneous active powers delivered to the ac grids by VSC1 and VSC2, respectively. The variables p_{cm} and p_Δ represent the common and differential powers, respectively. The main advantage of this representation is that active power that remains in the link is related to p_{cm}, while active power flowing from one grid to another is related to p_Δ [20]. The proposed controller will take advantage of this property to provide a fast and accurate control of the dc-link voltage while providing an effect similar to a friction between the two equivalent grids.

The output powers of the HVDC-link (p_{o1} and p_{o2}) can be obtained by manipulating the differential and common power expressions, (1) and (2), yielding:

$$p_{o1} = p_\Delta - p_{cm}/2, \qquad (3)$$
$$p_{o2} = -p_\Delta - p_{cm}/2. \qquad (4)$$

These expressions will be used later to calculate the power references for each VSC in terms of the common and differential power references.

C. Power System Modelling

The swing equation of generator 1 (the same equation can be used for generator 2) can be written as follows [21]:

$$2H_1 \frac{d\Delta\omega_1}{dt} = \Delta P_{m1} - \Delta P_{e1} - D_1\Delta\omega_1, \qquad (5)$$
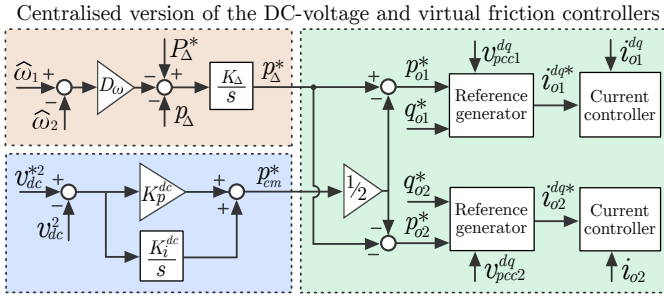
Fig. 2. Block diagram of the centralised virtual friction controller: (orange) Power controller and virtual friction, (blue) dc voltage controller, and (green) internal controllers and reference generation.

where Δ is the incremental operator, H_1 is the inertia constant, D_1 is the damping factor, ω_1 is the angular frequency, P_{m1} is the mechanical power supplied by the turbine and P_{e1} is the electrical power demanded by the network. The mechanical power (P_{m1}) is controlled by using a speed governor that can be represented as a first-order low-pass-filter [1],

$$P_{m1} = P^* + R_1/(T_1 s + 1) \cdot (\omega^* - \omega_1), \tag{6}$$

where R_1 is the frequency droop coefficient, and T_1 is a time constant that models the delayed response of the turbine actuator [21]. Furthermore, P^* and ω^* are the active power and angular frequency set points, respectively.

III. CENTRALISED VIRTUAL FRICTION CONTROLLER

Fig. 2 shows the block diagram of the centralised implementation of the proposed controller, where each block is explained in the following subsections. For this case, it is assumed that the measurements of both terminals are available to a common controller.

A. Centralised Virtual Friction

Fig. 2(a) shows the block diagram of the virtual friction controller. The differential power (p_Δ) is mainly related to the active power exchange between grids if losses and energy stored in the LCL filters of the terminals are neglected. Therefore, the variable p_Δ will be manipulated in order to provide virtual friction between ac networks:

$$p_\Delta^* = (K_\Delta/s) \cdot (P_\Delta^* - p_\Delta + D_\omega(\hat{\omega}_1 - \hat{\omega}_2)). \tag{7}$$

The hat "ˆ" refers to estimated (for example, by a PLL), P_Δ^* is the differential power set point, and D_ω is the equivalent mechanical friction.

If the transient response of the differential-power controller is significantly faster than that of the equivalent generators (G1 and G2), its dynamics can be neglected for system-level studies. Thus, the differential power can be expressed as:

$$p_\Delta = P_\Delta^* + B_\omega(\hat{\omega}_1 - \hat{\omega}_2). \tag{8}$$

If power losses are neglected, the swing equations of both equivalent generators can be expressed in terms of the HVDC-link active powers. Therefore, by substituting (3) and (4) in

(5) (and the same equation for G2), the swing equations of the generators become:

$$2H_1 \frac{d\omega_1}{dt} = P_{m1} + P_\Delta^* + D_\omega(\hat{\omega}_1 - \hat{\omega}_2) - p_{cm}/2 - D_1\omega_1, \tag{9}$$

$$2H_2 \frac{d\omega_2}{dt} = P_{m2} - P_\Delta^* - D_\omega(\hat{\omega}_1 - \hat{\omega}_2) - p_{cm}/2 - D_2\omega_2. \tag{10}$$

It can be seen that the coefficient D_ω multiplies the frequency difference between both ac grids and its effect is equivalent to that of a mechanical friction.

B. Centralised DC-Voltage Controller

Fig. 2(b) shows the block diagram of the dc-voltage controller. By neglecting losses and energy stored in the elements of LCL filters, the dynamic equation that models the energy stored in the dc capacitor can be written as [20]:

$$(C'_{dc}/2) \cdot dv_{dc}^2/dt = p_{cm}. \tag{11}$$

The common power (p_{cm}) is directly related to the energy stored in the dc capacitor. Therefore, a classical PI controller can be applied to control the dc voltage by manipulating the common-power reference:

$$p_{cm}^* = (K_p^{dc} + K_i^{dc}/s) \cdot (v_{dc}^{*2} - v_{dc}^2), \tag{12}$$

where K_p^{dc} and K_i^{dc} are the controller gains.

C. Reactive Power Controller

Reactive power injection of each terminal can be controlled independently. Therefore:

$$q_o^* = (K_Q/s) \cdot (Q_o^* - q_o + D_V(|\vec{v}_{pcc}^*| - |\vec{v}_{pcc}|)), \tag{13}$$

where Q_o^* is the reactive power set point, q_o is the instantaneous value of the reactive power, D_V is the reactive power-voltage droop coefficient, and $|\vec{v}_{pcc}^*|$ and $|\vec{v}_{pcc}|$ are the module of the PCC voltage space vector and its reference value, respectively.

D. Centralised Power Reference Generation

Fig. 2(c) shows the block diagram of the power reference generator. The proposed controller will generate the reference values (p_Δ^* and p_{cm}^*). Active power references (p_{o1}^* and p_{o2}^*) are obtained by using the power expressions (3) and (4). Reactive power references can be set independently (q_{o1}^* and q_{o2}^*). Current references are generated by using the output power of each terminal, independently. Therefore, for one terminal, the dq-axes current references can be written as [22]:

$$i_o^{d*} = p_o^*/v_{pcc}^d, \quad i_o^{q*} = -q_o^*/v_{pcc}^d. \tag{14}$$

IV. DECENTRALISED VERSION OF THE CONTROLLER

Fig. 3 shows the decentralised control implementation for VSC1. The same scheme (with the notation adapted) is used for VSC2. The blocks in the control system are described in the following subsections, except the reactive power controller,

Decentralised version of the DC-voltage and virtual friction controllers
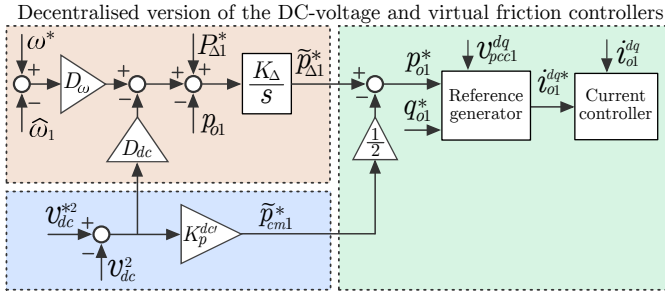
Fig. 3. Block diagram for the decentralised implementation of the dc-voltage and the point-to-point virtual friction controllers for VSC1: (orange) Power and virtual friction controller, (blue) dc-voltage controller and (green) current controller and reference generator.

Fig. 4. Simplified block diagram of the two power network connected via the virtual friction.

which is the same already explained for the centralised controller. For the decentralised controller, it is assumed that only the measurements of one terminal are accessible in real-time.

A. Decentralised Virtual Friction

In order to implement a decentralised controller, two new variables, called $\tilde{p}_{\Delta 1}^*$ and $\tilde{p}_{\Delta 2}^*$, are defined. For the terminal one, this new variable is defined as follows:

$$\tilde{p}_{\Delta 1}^* = (K_\Delta/s) \cdot (P_{\Delta 1}^* - p_{o1} + D_\omega'(\omega^* - \hat{\omega}_1) + \\ - D_{dc}(v_{dc}^{*2} - v_{dc}^2)), \quad (15)$$

where D_ω' is a frequency droop, D_{dc} is a droop coefficient for the dc-voltage that has been added to the original expression of p_Δ^* in (7). Its main objective is to share information between terminals regarding mismatches in $\tilde{p}_{\Delta 1}^*$ and $\tilde{p}_{\Delta 2}^*$.

B. Decentralised DC-Voltage Controller

Since both VSCs share the control of the dc-voltage, the use of two integral actions like (12) should be avoided [23]. Therefore, the PI controller was replaced by a P controller, yielding:

$$\tilde{p}_{cm1}^* = K_p^{dc'} \cdot (v_{dc}^{*2} - v_{dc}^2). \quad (16)$$

where $K_p^{dc'}$ is the dc controller gain.

In steady state, if (15) and the version of (15) for the terminal 2 are subtracted and divided by two, the following steady-state relationship is obtained:

$$\underbrace{(P_{\Delta 1}^* - P_{\Delta 2}^*)/2}_{p_\Delta^*} - \underbrace{(p_{o1} - p_{o2})/2}_{p_\Delta} - (D_\omega'/2)(\omega_1 - \omega_2) = 0. \quad (17)$$

It can be seen that, if the droop coefficients of both VSCs have the same values, the frequency droop (D_ω') is the equivalent virtual friction seen between the two generators.

C. Decentralised Power Reference Generation

The active-power references for VSC1 and VSC2 (p_{o1}^* and p_{o2}^*) can be calculated by using the method already proposed for the centralised controller. However, the original values of

p_Δ and p_{cm} should be replaced by the modified values of the decentralised controller, $\tilde{p}_\Delta$ and $\tilde{p}_{cm}$. Therefore:

$$p_{o1}^* = \tilde{p}_{\Delta 1}^* - \tilde{p}_{cm1}^*/2, \quad (18)$$
$$p_{o2}^* = \tilde{p}_{\Delta 2}^* - \tilde{p}_{cm2}^*/2. \quad (19)$$

V. CONTROL SYSTEM DESIGN

In this section, the parameters of the centralised and decentralised controllers are designed.

A. Active and Reactive Controllers Design

The design procedure is the same for the centralised and the decentralised version of the secondary controller. In order to avoid interactions between inner control loops and the proposed controller, their time constants should be sufficiently separated. If this condition is met, the input-output transfer function of the active power controller for the terminal one is, approximately:

$$\frac{\tilde{P}_{\Delta 1}(s)}{P_{\Delta 1}^*(s)} = \frac{1}{s/K_{\Delta 1} + 1}. \quad (20)$$

Following a similar approach for the reactive power controller:

$$\frac{Q_{o1}(s)}{Q_{o1}^*(s)} = \frac{1}{s/K_{Q1} + 1}. \quad (21)$$

Therefore, the frequency of the closed-loop poles can be selected with $\omega_p = K_{\Delta 1}$ and $\omega_{Q1} = K_{Q1}$.

B. DC-Voltage Controllers Design

For the centralised controller, the gains of the dc-voltage controller can be designed as a classical PI controller. The natural frequency and damping factor of the second-order closed-loop system can be selected as:

$$K_p^{dc} = \zeta \omega_n C_{dc}', \quad K_i^{dc} = \omega_n^2 C_{dc}'/2. \quad (22)$$

For the decentralised controller, the gain of the dc-voltage controller can be designed as a P controller where the cut-off frequency of the first-order closed-loop system can be selected by using the following expression:

$$K_p^{dc'} = \omega_p C_{dc}'. \quad (23)$$

VI. CASE STUDY AND ANALYTICAL RESULTS

A. Case Study

The parameters of the equivalent generators were set to $H_1 = 1/5$ pu, $H_2 = 1/200$ pu, $D_1 = 0$, $D_2 = 0$, $R_1 = 0.5$ pu,
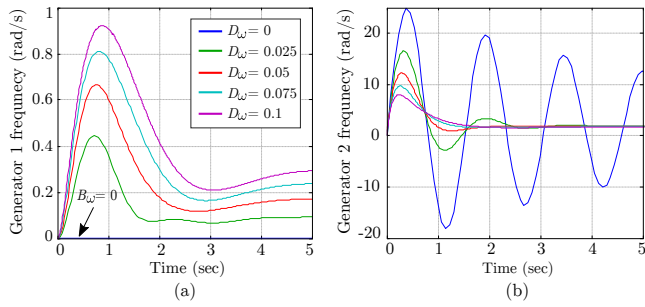
Fig. 5. Simulation results: Transient response of the two power networks connected via a virtual friction when a step-change was applied to the electrical power of G2 P_{e2}. (a) Angular frequency of G1, (b) angular frequency of G2, and (c) power transfer between ac networks.

$R_2 = 0.5$ pu, $T_1 = 0.5$ s and $T_2 = 3$ s. By using these parameters, the damping factor of generator G1 is $\zeta = 0.63$, while the damping factor of generator G2 is $\zeta = 0.04$.

B. Control System Design

The control parameters have been designed according to the procedure described in Section V. Conventional PI controllers were used for the inner current controllers, and they are designed to achieve a settling time of $t_{set} < 5$ ms and an overshoot $M_p < 10\%$. The dc-voltage controller is designed to have $\omega_p = 300$ rad/s. The active and reactive power controllers are designed to have $\omega_p = 2\pi 10$ rad/s and $\omega_{Q1} = \omega_{Q2} = 2\pi 10$ rad/s. The reactive power-voltage droop coefficients are determined by the application requirements. Both VSCs have the same droop values, $D_V = 0.01$ pu. The frequency droop coefficient (virtual friction) is set to $D_\omega = 0.05$. The dc-voltage droop coefficient (D_{dc}) can the adjusted to achieve the desired relation between frequency and dc-voltage deviation. In this case, the dc-voltage droop coefficient was set to $D_{dc} = 0.1$.

C. Analysis of the Virtual Friction Concept

The simplified model in Fig. 4 was used to analyse the performance of the proposed controller. Fig. 5 shows the transient response of the two networks connected by a virtual friction when a step-change was applied to the electrical power demanded by network 2 (P_{e2}) and for different values values of D_ω. For $D_\omega = 0$ (blue lines), the two networks are decoupled and the step change excited the low-frequency resonance of G2, producing a poorly damped frequency oscillation (Fig. 5(b)). For $D_\omega > 0$, the two networks are coupled by the virtual friction (HVDC-link) and the impact of the disturbance can be mitigated. When D_ω increases, the coupling effect increases and network 1 supports network 2 when a disturbance takes place, damping the low-frequency resonance.

Therefore, it has been shown that the parameter D_ω (D'_ω) has an effect equivalent to a mechanical friction connected between generators G1 and G2.
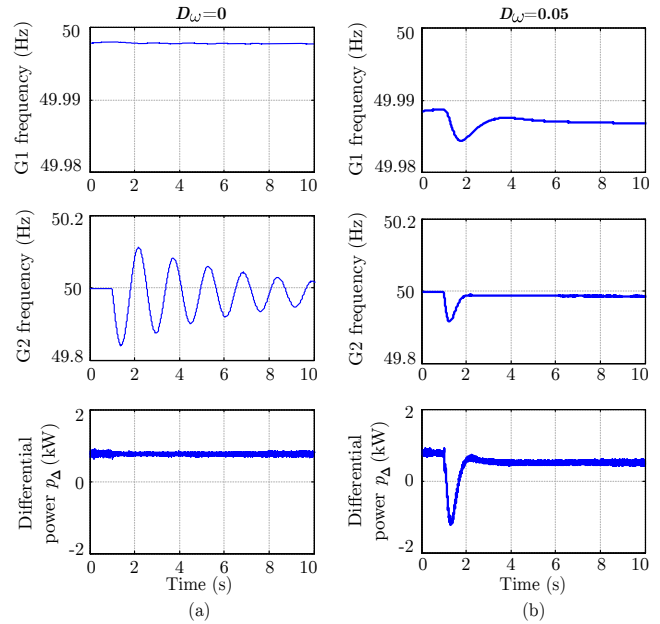
Fig. 6. Simulation results: Transient response of the two power networks connected via the centralised implementation of the virtual friction when a step-change was applied to the electrical power of G2. (a) The virtual friction was $D_\omega = 0$, and (b) the virtual friction was $D_\omega = 0.05$
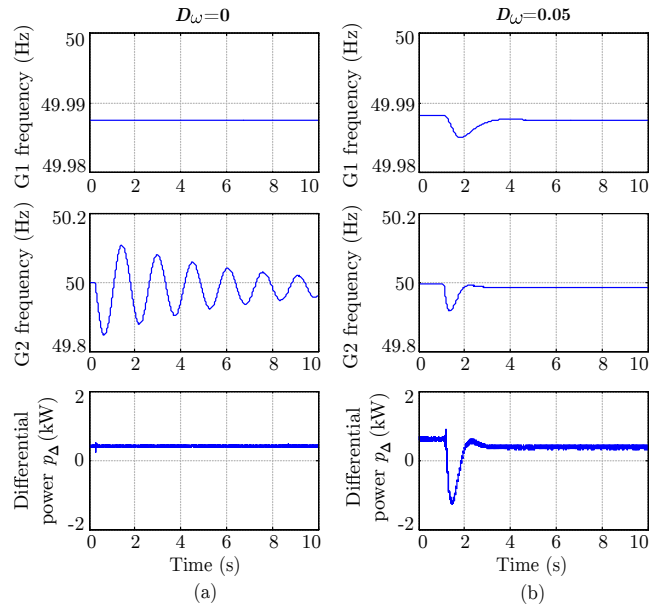
Fig. 7. Experimental results: Transient response of the two power networks connected via the decentralised implementation of the virtual friction when a step-change was applied to the electrical power of G2 P_{e2}: (a) the virtual friction was $D'_\omega = 0$, and (b) the virtual friction was $D'_\omega = 0.05$

VII. RESULTS

A. Prototype Description

The proposed control system was experimentally validated in the Smart Energy Integration Lab (SEIL) [24]. The nominal grid voltage and frequency of both ac grids is 400 V and 50 Hz. The ac grids represented are emulated by using two 75 kVA VSC with LCL filter ($S_B = 75$ kVA). A fourth

order synchronous generator model is assumed which includes the mechanical shaft, the speed governor and the exciter to control the rotor field. Two 15 kVA converters in back-to-back configuration are used as the VSC-HVDC interconnection.

B. Centralised Controller Results

Fig. 6(a) shows the transient response of the system when a step change was applied to the electrical power demanded by the local load of G2 P_{e2}, and the virtual friction was disabled ($D_\omega = 0$). It can be seen that generator G2 has a poorly damped resonance. The differential power is not affected by the step change in the power. Fig. 6(b) shows the same experiment, but when the virtual friction was activated ($D_\omega = 0.05$). It can be seen that the resonance of G2 is now well damped, and the additional active power required to damp the resonance is taken from G1.

C. Decentralised Controller Results

Fig. 7(a) shows the transient response of the system when a step change was applied to the electrical power demanded by the local load of G2 P_{e2}, and the virtual friction was disabled ($D'_\omega = 0$). It can be seen that, when the load is connected, the generator exhibits a poorly damped resonance. Fig. 7(a) shows the transient response of the system when a step change was applied to the electrical power demanded by the local load of G2 P_{e2}, and the virtual friction was set to $D'_\omega = 0.05$. It can be seen that, when the load is connected, the frequency of G2 deviates. However, the virtual friction controller introduced an active power exchange between G1 and G2, and the differential power was modified. This active power exchange damped the low frequency oscillation.

VIII. CONCLUSION

In this paper, a controller for VSC-HVDC interconnections based on the virtual fiction concept has been presented. This concept has been introduced by using the differential and common powers of a VSC-HVDC link. Two versions of the controller have been proposed: a centralised and a decentralised implementation. The performance of the controller has been validated in simulation and on an experimental platform. The results showed the frequency oscillations in both ac networks can be damped at the same time by tuning the gain D_ω representing the virtual friction. It has been demonstrated that the decentralised version of the controller offered a similar performance compared to the centralised implementation. However, in this case the dc voltage varies during operation.

REFERENCES

[1] P. Kundur, N. Balu, and M. Lauby, *Power System Stability and Control*, ser. Discussion Paper Series. McGraw-Hill Education, 1994.

[2] A. Junyent-Ferre, Y. Pipelzadeh, and T. C. Green, "Blending hvdc-link energy storage and offshore wind turbine inertia for fast frequency response," *IEEE Tran Sustainable Energy*, vol. 6, no. 3, pp. 1059–1066, July 2015.

[3] M. A. Elizondo, R. Fan, H. Kirkham, M. Ghosal, F. Wilches-Bernal, D. Schoenwald, and J. Lian, "Interarea oscillation damping control using high-voltage dc transmission: A survey," *IEEE Tran Power Systems*, vol. 33, no. 6, pp. 6915–6923, Nov 2018.

[4] E. Romero-Ramos, A. Gomez-Exposito, A. Marano-Marcolini, J. M. Maza-Ortega, and J. l. Martinez-Ramos, "Assessing the loadability of active distribution networks in the presence of dc controllable links," *IET Gen, Trans Distri*, vol. 5, no. 11, pp. 1105–1113, Nov 2011.

[5] J. Fang, H. Li, Y. Tang, and F. Blaabjerg, "On the inertia of future more-electronics power systems," *IEEE Journal of Emerging and Selected Topics in Power Electronics*, pp. 1–1, 2018.

[6] J. P. Sucena-Paiva and L. L. Freris, "Stability of a d.c. transmission link between strong a.c. systems," *Proceedings of the Institution of Electrical Engineers*, vol. 120, no. 10, pp. 1233–1242, October 1973.

[7] C. Zou, H. Rao, S. Xu, Y. Li, W. Li, J. Chen, X. Zhao, Y. Yang, and B. Lei, "Analysis of resonance between a vsc-hvdc converter and the ac grid," *IEEE Tran Power Elec*, vol. 33, no. 12, pp. 10 157–10 168, 2018.

[8] L. Zeni, R. Eriksson, S. Goumalatsos, M. Altin, P. Srensen, A. Hansen, P. Kjr, and B. Hesselbk, "Power oscillation damping from vschvdc connected offshore wind power plants," *IEEE Tran Power Del*, vol. 31, no. 2, pp. 829–838, April 2016.

[9] H. Latorre and M. Ghandhari, "Improvement of power system stability by using a vsc-hvdc," *International Journal of Electrical Power & Energy Systems*, vol. 33, no. 2, pp. 332 – 339, 2011.

[10] J. Zhu, C. D. Booth, G. P. Adam, A. J. Roscoe, and C. G. Bright, "Inertia emulation control strategy for vsc-hvdc transmission systems," *IEEE Transactions on Power Systems*, vol. 28, no. 2, pp. 1277–1287, 2012.

[11] M. Guan, W. Pan, J. Zhang, Q. Hao, J. Cheng, and X. Zheng, "Synchronous generator emulation control strategy for voltage source converter (vsc) stations," *IEEE Transactions on Power Systems*, vol. 30, no. 6, pp. 3093–3101, 2015.

[12] R. Aouini, B. Marinescu, K. B. Kilani, and M. Elleuch, "Stability improvement of the interconnection of weak ac zones by synchronverter-based hvdc link," *Electric Power Systems Research*, vol. 142, no. Supplement C, pp. 112–124, 2017.

[13] L. Huang, H. Xin, H. Yang, Z. Wang, and H. Xie, "Interconnecting very weak ac systems by multiterminal vsc-hvdc links with a unified virtual synchronous control," *IEEE Journal of Emerging and Selected Topics in Power Electronics*, vol. 6, no. 3, pp. 1041–1053, Sep. 2018.

[14] Y. Shen, W. Yao, J. Wen, H. He, and W. Chen, "Adaptive supplementary damping control of vsc-hvdc for interarea oscillation using grhdp," *IEEE Tran Power Systems*, vol. 33, no. 2, pp. 1777–1789, March 2018.

[15] B. Pierre, R. Elliott, D. Schoenwald, J. Neely, R. Byrne, D. Trudnowski, and J. Colwell, "Supervisory system for a wide area damping controller using pdci modulation and real-time pmu feedback," in *2016 IEEE Power and Energy Society General Meeting*, 2016, pp. 1–5.

[16] P. Agnihotri, A. Kulkarni, A. M. Gole, B. A. Archer, and T. Weekes, "A robust wide-area measurement-based damping controller for networks with embedded multiterminal and multiinfeed hvdc links," *IEEE Tran Power Systems*, vol. 32, no. 5, pp. 3884–3892, 2017.

[17] Y. Phulpin, "Communication-free inertia and frequency control for wind generators connected by an hvdc-link," *IEEE Tran Power Systems*, vol. 27, no. 2, pp. 1136–1137, May 2012.

[18] X. Liu and A. Lindemann, "Control of vsc-hvdc connected offshore windfarms for providing synthetic inertia," *IEEE Journal of Emerging and Selected Topics in Power Electronics*, vol. 6, no. 3, pp. 1407–1417, Sep. 2018.

[19] J. Rafferty, L. Xu, Y. Wang, G. Xu, and F. Alsokhiry, "Frequency support using multi-terminal hvdc systems based on dc voltage manipulation," *IET Renewable Power Gen*, vol. 10, no. 9, pp. 1393–1401, 2016.

[20] A. Rodríguez-Cabero, M. Prodanovic, and J. Roldán-Pérez, "Full-state feedback control of back-to-back converters based on differential and common power concepts," *IEEE Tran Ind Elec*, pp. 1–1, 2018.

[21] H. Bevrani, B. François, and T. Ise, *Microgrid Dynamics and Control*. Wiley, 2017.

[22] H. Akagi, Y. Kanazawa, and A. Nabae, "Instantaneous reactive power compensators comprising switching devices without energy storage components," *IEEE Tran Ind Appli*, vol. IA-20, no. 3, pp. 625–630, May 1984.

[23] A. Kirakosyan, E. F. El-Saadany, M. S. E. Moursi, and K. Al Hosani, "DC Voltage Regulation and Frequency Support in Pilot Voltage Droop-Controlled Multiterminal HVdc Systems," *IEEE Trans Power Del*, vol. 33, no. 3, pp. 1153–1164, 2018.

[24] M. Prodanovic, A. Rodríguez-Cabero, M. Jiménez-Carrizosa, and J. Roldán-Pérez, "A rapid prototyping environment for dc and ac microgrids: Smart energy integration lab (seil)," in *ICDCM 2017*, June 2017, pp. 421–427.